COBEM 2023 27TH INTERNATIONAL CONGRESS OF MECHANICAL ENGENEERING

ABCM Brazilian Society of Mechanical Sciences and Engineering
27th ABCM International Congress of Mechanical Engineering
December 04-08, 2023, Florianópolis-SC, Brazil

# COB-2023-0537
# PARTICLE TRACKING VELOCIMETRY (PTV) MEASUREMENT TECHNIQUE FOR AN EXPERIMENTAL INVESTIGATION OF SURROUNDING AIR BEHAVIOR IN ETHANOL SPRAY DEVELOPMENT

**Victor Cupola Ganino**
**Rafael Hauckewitz Todaro**
**Rafael da Cruz Ribeiro Berti**
**Guenther Carlos Krieger Filho**
**Antonio Luis Pacifico**
Escola Politécnica da Universidade de São Paulo - Avenida Professor Mello Moraes, 2231 - Butantã, São Paulo - SP
victor.cupola@usp.br, todaro@usp.br, rafaelcrberti@gmail.com, guenther@usp.br, alpacifi@usp.br.

***Abstract.*** *Sustainable internal combustion engines associated with lower fuel consumption and lower levels of pollutant emissions are in demand for the next generation of vehicles. Ethanol fuel is a good alternative to meet market demands when equipped with a direct injection system. In the development of the spray formation, understanding the dynamics of the inlet surrounding air is fundamental to establishing a more robust understanding of the internal combustion chamber environment. Fluid velocity measurement techniques are widely used, and the most reliable techniques nowadays are non-intrusive optical measurements, such as Particle Image Velocimetry (PIV) and Particle Tracking Velocimetry (PTV). Despite the popularity of PIV, the PTV technique is gaining attention with new algorithms developed to handle higher-seeded flows, as its demands were specific for evaluating sparsely seeded flows. This work aims to advance the studies previously carried out on ethanol spray development using the Isothermal Ethanol Spray Chamber (IESC). The experimental methodology operated with a constant flow chamber with optical access to the spray's surrounding environment. The injection pressure of the spray was 60 bar, and the average air mass flow was 0.066 kg/s. Air flow doped with tracer particles and captured with recording cameras represented the surrounding air movement. The objective was to use the experimental data obtained with the PIV technique and compare it with the PTV technique using the same raw images of the surrounding air of the spray. The PIV measurements showed excessive noise in areas of low seeding segments or high-velocity gradients of the flow. Through image pre-processing, it was possible to achieve a 150% better signal-to-noise ratio (SNR). The results were averaged, and outlier detection averaged about 15%. Analyses were also conducted to ensure the quality of the resultant flow field with peak-locking analysis. The PTV vector field provided valuable information, with a global velocity magnitude ranging from 2 to 15 m/s. The horizontal and vertical velocity components of these vectors were determined and related to the spray development stage and injection pressures. Recirculation structures, air drag into spray cavities, and global drag behind the spray could be observed using the PTV technique. The two-phase flow was challenging due to differences in particle concentration, but the PTV provided information about air movement in the experimental conditions representative of real engine operation, except for low rotational speed and high load conditions.*

***Keywords:*** *Particle Tracking Velocimetry measurement, Air-spray interaction, Ethanol.*

## 1. INTRODUCTION

Reducing gas pollutant emissions to preserve the environment has driven countries to seek alternative solutions for their dependency on fossil fuels. Brazil has a solid alternative in the National Program of Ethanol Production, launched in 1975 (Proalcool). The program focused on encouraging biofuel consumption with the aim of reducing dependence on petroleum and its derivatives. Despite efforts to address mobility issues, the OECD (Organization for Economic Cooperation and Development) predicts an increase in individual transport in the coming years. In response to the Proalcool initiative, the domestic market introduced *flex-fuel* technology in 2003. This technology not only provided flexibility in regulating petroleum product prices but also enabled automotive consumption of ethanol, leading to a reduction in $CO_2$ emissions. Sales of new vehicles in Brazil equipped with *flex-fuel* technology have been on the rise, with ethanol playing a fundamental role due to its unique characteristics when used in ignition engines [Zabeu (2019)].

Direct Injection Spark Ignition (DISI) engines are crucial for reducing $CO_2$ emissions. According to Baumgarten (2006), DISI engines offer the highest potential for reducing fuel consumption and, consequently, $CO_2$ emissions compared to other techniques. In comparison with similar port-fuel injection engines, direct injection systems can achieve a reduction in fuel consumption of about 15% to 25% in part-load conditions [Baumgarten (2006), Berti (2018)].

In the pursuit of sustainable solutions, Brazil has a unique opportunity to establish hybrid electric/ethanol fleets, as highlighted by Todaro (2020). Therefore, injection strategies for the spray development of ethanol fuel are essential

for internal combustion engines equipped with direct injection systems. However, knowledge about air-fuel mixture formation for this type of engine is still limited. To better characterize the surrounding airflow of the spray, Berti (2018) conducted Particle Image Velocimetry (PIV) measurements, while Todaro *et al.* (2020) proposed an optimization approach to enhance the vector field's reliability using signal-to-noise ratio maximization as the objective function. Nevertheless, the two-phase gas-spray flow presented some challenges that may reduce the representativeness of the results, such as inadequate particle concentration in some areas and high image noise due to strong light scattering from the spray. The recorded spray event showed an average particle density of 0.025 particles per pixel (ppp). These issues have prompted the search for alternative measurement methods.

Particle Tracking Velocimetry (PTV) is a flow measurement technique originally designed for sparsely seeded flows. However, PTV algorithms capable of handling a larger number of particles have been developed. The measurement process is similar to PIV, especially in terms of image acquisition and light scattering techniques. Nevertheless, PIV uses an interrogation window to subsample an image pair, whereas PTV analyzes individual particles to identify the velocity field [Raffel *et al.* (2007), Dabiri and Pecora (2019)]. Additionally, Janke *et al.* (2020) proposed a PTV measurement algorithm with the suggested optimal seeding density ranging between 0.0025 and 0.05 for the chosen processing parameters, where at least 90% of all detected particles were matched validly.

This paper presents a PTV analysis of the gas phase in the two-phase air-spray development near the spray tip, where PIV exhibited a lower signal-to-noise ratio. The PTV analysis was introduced to address the lack of information provided in some areas by the PIV technique. Furthermore, this work provides the PTV velocity field for the surrounding air at different stages of spray development and reports coherence between the measured velocity and that found by the PIV measurement.

## 2. METHODOLOGY

### 2.1 Experimental Apparatus

The interaction between the surrounding air and the spray was conducted inside a specially designed chamber to replicate near-ambient conditions where the spray encounters airflow during the intake stroke inside the cylinder. The chamber's ambient pressure was set at 1 bar, representing the typical conditions of a real engine cycle, except for situations of low rotational speed or high-performance demands when stratified injection is applied.

The chamber, known as the Isothermal Ethanol Spray Chamber (IESC), is divided into two sections. The first section features a cylindrical geometry with a diameter of 100 mm and a length of 500 mm, constructed from aluminum. In this section, inlet air is introduced through the top entrance via a blower rotating at a constant speed of 600 rotations per minute. The average nominal mass flow rate was 0.066 kg/s, resulting in a Reynolds number of $4.22 \times 10^4$, calculated using the hydraulic diameter of the IESC. To ensure homogeneous distribution, the mixture of air and particle tracers occurs at a certain distance. At the end of this section, two radially perforated plates with equally spaced 4.0 mm holes are positioned to limit turbulence levels to an integral scale length similar to that found inside internal combustion engine cylinders. In the center of these perforated plates, a multi-hole GDI (Gasoline Direct Injection) Delphi injector is located to provide sequential pressurized spray events. Ethanol is injected at 60 ± 3 bar in a sequence of 15 injections, with each injection lasting 3 ms (the time between Start Of Injection, SOI, and End Of Injection, EOI).

The second section of the IESC is the optical accessible section, composed of four quartz windows measuring 85×136 mm each, with an equal thickness of 3.14 mm, arranged in a square configuration to minimize light distortions. To reduce light scattering, the aluminum parts of this section are anodized and coated with black. The size of the windows allows for full visualization of spray development and its interaction with the controlled inlet airflow. Figure 1 illustrates the IESC and its internal components.

The air is doped with tracer particles and represents the continuous phase, with Rhodamine B fluorescent particles dissolved in Propylene Carbonate representing the airflow phase, and spray droplets representing the liquid phase. Seeding particles are generated by a Laskin nozzle. Previous experiments using Phase-Doppler Interferometry (PDI) demonstrated that the tracers used have a Sauter Mean Diameter (SMD) of 3.0 $\mu$m, ensuring that particles follow the flow with minimal slip, as described by Melling (1997). In some cases, droplets from the spray may serve as natural tracer particles, and thus, the liquid phase is studied by recording the elastic scattering of the dispersed ethanol droplets.

The light source employed is a double-cavity Nd: YLF laser beam with a wavelength of 527 nm and an energy of 15 J per pulse. This light source generates a planar sheet measuring 50 mm in height and 1 mm in thickness. Both phases, the continuous and the dispersed, are recorded simultaneously using two Phantom v3.11 cameras manufactured by Vision Research Inc. These cameras are equipped with 1280×800 pixel CMOS (Complementary Metal Oxide Semiconductor) sensors with 12-bit resolution. They are positioned orthogonally to the light sheet. One camera captures the light scattered by the droplets of the spray, which occurs at the laser wavelength. To do so, this camera is equipped with a set of filters with a bandpass centered at 527 ± 5 nm and neutral filters to attenuate the visible spectra. The other camera records the air tracer particles using a set of optical filters containing a sequence of dichroic beamsplitter filters and three longpass filters.

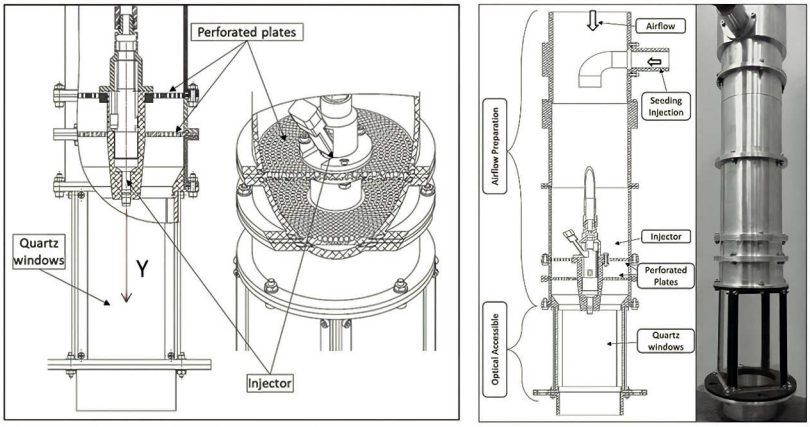


Figure 1. The Isothermal Spray Chamber. The left figure is a partial section that shows in details the perforated plates and the injector. The right figure is a comparison between the complete section view of the chamber and its photograph. Adapted from Berti (2018).

To synchronize the injection of ethanol with the cameras, a control system was developed. Figure 2 illustrates the experimental setup for image acquisition.

All parameters defining the adopted configurations were independently controlled, and the full-scale length of the turbulent flow was 3.5 mm. The acquisition rate was 8000 Hz with an interframe time interval of 20 $\mu$s. For each case, images were recorded in 17 sequences, with each sequence containing 15 injection events. This resulted in 255 spray injection cycles under the same conditions, yielding 14001 images from each injection event sequence. All images were recorded as a pixel matrix of 360×512 pixels, equivalent to $20.4 \times 29$ mm (mapping scale parameter of 0.0566 mm/pixel), with grayscale values and 12 bits of resolution. The spatial resolution of the imaging system was 59 $\mu$m/pixel. The Field Of View (FOV) encompasses the region to the left of the spray's symmetry axis.

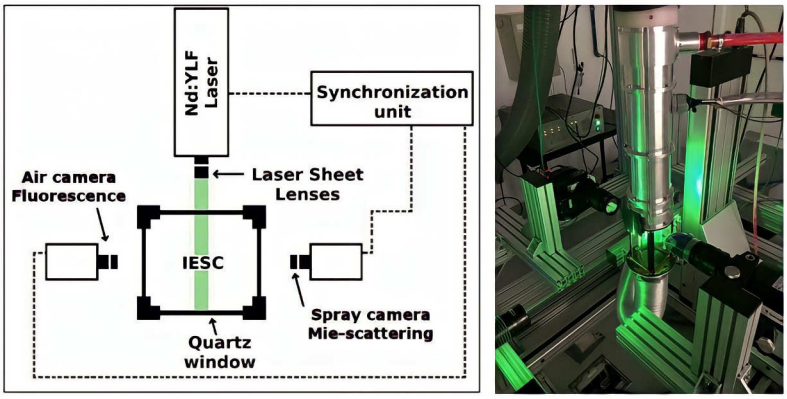


Figure 2. Schematic of the experimental arrangement used for two phase acquisition. The left figure shows a camera disposal and the synchronizing unit schematic. The right figure is a photograph of the camera disposal and the IESC. Adapted from Berti (2018)

### 2.2 PTV application

Particle Tracking Velocimetry (PTV) measurement has gained significant attention due to the development of automatic particle tracking algorithms, which offer spatial resolutions comparable to tomographic Particle Image Velocimetry (PIV) for 3D measurements in continuous flows [Schanz *et al.* (2013)]. PTV involves individually tracking particles and does not suffer from spatial averaging, thus allowing for the avoidance of bias errors [Kahler *et al.* (2012)]. According to Fuchs *et al.* (2017), spatial resolution can be improved down to the sub-pixel level for mean velocity fields.

Despite its advantages, the PTV method has some drawbacks, including the use of complex iterative algorithms. These challenges were addressed by Fuchs *et al.* (2017) and further extended by Janke *et al.* (2020), who proposed a reliable tracking procedure based on double-frame recordings at relatively high seeding concentrations. For the double-frame approach, Janke *et al.* (2020) introduced a simple nearest neighbor matching method and a technique capable of handling higher particle densities, known as histogram matching. This approach not only reduced processing time but also

enabled the reliable tracking of particles at particle densities of up to 0.06 particles per pixel ($N_{ppp}$) from double-frame data. However, it's important to note that this algorithm requires a clean dark background and bright particle images to effectively locate and track the particles, necessitating the use of a pre-processing routine.

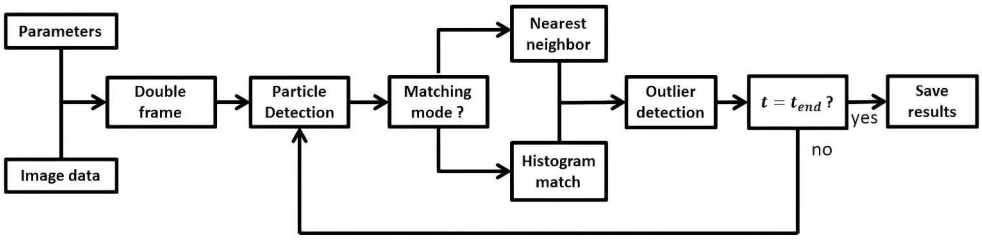


Figure 3. Schematic representation of the main processing routine. Adapted from Janke *et al.* (2020).

The pre-processing routine, as proposed by Todaro (2020), was designed to enhance identification and tracking strategies while removing background noise present in the recordings. This process exclusively employs spatial filters and involves a straightforward numerical procedure.

The pre-processing begins with an RMS (Root Mean Square) spatial filter, primarily aimed at eliminating signal noise and particles with smaller diameters, as recommended by Raffel *et al.* (2007). This filtering technique utilizes standard deviation calculations based on a $3 \times 3$ kernel.

Subsequently, a Gaussian filter is applied to enhance the shape of the particles. It uses a standard deviation of $0.1$ ($\sigma = 0.1$) and a $3 \times 3$ kernel. This step helps reduce noise while preserving the integrity of homogeneous regions.

Additionally, a Subtract Sliding Minimum (SSM) filter is employed to ensure a significant contrast between the particles and the background. This filter is applied to all matrices within a $50 \times 50$ kernel.

To address Bright Spots (BS) and prevent them from affecting the processing of suitable particles, an Intensity Capping method developed by Shavit *et al.* (2007) is applied.

Finally, another round of Gaussian filtering is performed, this time with a standard deviation of $1$ ($\sigma = 1$). This series of pre-processing steps collectively improves the quality of the recorded data, making it more suitable for subsequent analysis and tracking.

The processing and post-processing routine were developed by Janke *et al.* (2020), which is a MATLAB® algorithm to apply PTV measurement called Part2Track. The algorithm can resolve time-resolved and double-frame PTV, however, only double-frame PTV was applied in the present work. The figure 3 shows a schematic representation of the processing routine.

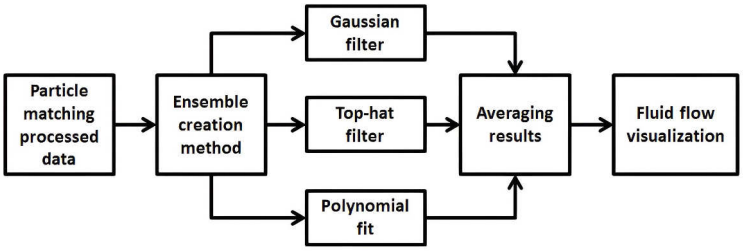


Figure 4. Post-processing schematic view

The particle detection method, known as 'blob detection,' as adopted from Heyman (2019), allows for sub-pixel accurate detection of tracer particles. This method comprises a series of steps, beginning with the Laplacian of Gaussian image filtering technique, followed by Gaussian interpolation of the particle peak intensities. This approach has proven effective in accurately identifying and locating tracer particles.

To handle higher particle densities, a matching technique known as 'histogram matching' is employed. Initially developed by Fuchs *et al.* (2017) and extended by Janke *et al.* (2020), this method focuses on finding the smallest absolute deviation from possible particle displacements and their neighboring positions as calculated by histograms. An additional step involves a universal outlier detection process, enhancing the overall quality of the displacement field, as proposed by Westerweel and Scarano (2005). Furthermore, this method has been generalized by Duncan *et al.* (2010) to work with scattered Particle Tracking Velocimetry (PTV) data, further enhancing the accuracy of the displacement field reconstruction.

To improve resolution and accuracy, the ensemble particle tracking velocimetry process is utilized. This process involves binning methods to interpolate scattered data onto a regular grid, offering adjustable grid sizes and interrogation windows. Two binning methods are implemented: Gaussian-weighted binning and binning based on second-degree

polynomial interpolators, as described in Aguera *et al.* (2016) and Janke *et al.* (2020). Following the ensemble process, velocity components are expressed as second-order polynomials, providing precision, as outlined by Aguera *et al.* (2016).

Figure 4 presents a schematic view sequence of the post-processing steps. For further details about the Part2Track method, please refer to Janke *et al.* (2020).

To ensure the quality of the results, a peak locking analysis was conducted in this study. Measurement uncertainties can be categorized into random errors and bias errors. While random errors can be mitigated through statistical analysis with a sufficiently large ensemble set, bias errors may persist even after averaging, as highlighted by Chen and Katz (2005). Peak locking error is a significant bias error that can occur when particle images are very small, leading to a shift in estimated displacement values toward the nearest integer pixel position [Raffel *et al.* (2018)]. To mitigate significant bias errors resulting from peak locking, it is crucial to have a particle image diameter of at least two pixels. The presence of peak locking can be detected by examining a displacement histogram, which will exhibit distortions when systematic errors outweigh random noise in displacement estimates. Additionally, the probability density function of peak locking will have peaks at integer pixel values, while sub-pixel displacements typically vary between 0 and 1. In cases of peak locking, the histogram will show higher counts near 0 and 1. The 'peak locking degree' is a parameter that quantifies the extent of peak locking, calculated by finding the minimum and maximum counts and evaluating it using

$$PD = 1 - \frac{N_{min}}{N_{max}} \tag{1}$$

where $PD$ represents the peak locking degree, $N_{min}$ is the minimum occurrence of a sub-pixel displacement in pixels, and $N_{max}$ is the maximum occurrence of a sub-pixel displacement in pixels. Higher values of the peak locking degree indicate a greater presence of bias error or peak locking error.

## 3. RESULTS AND DISCUSSIONS

### 3.1 Air flow velocities and flow structures

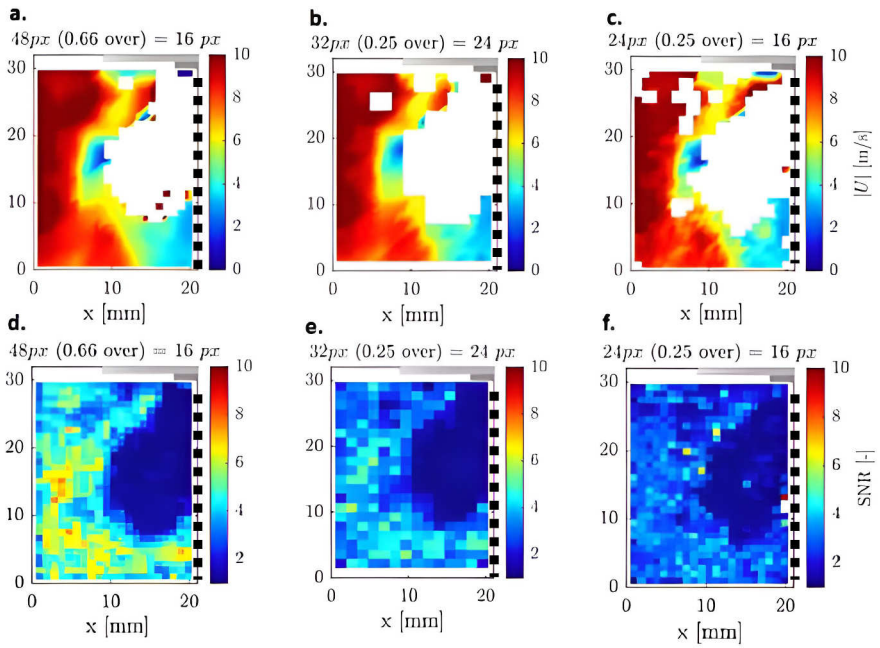


Figure 5. The black dashed line represents the spray centerline, where the spray tip is located in the superior right of the image. a. Velocity field with 0.66 overlapping on an interrogation window of 48 pixels. b. Velocity field with 0.25 overlapping on an interrogation window of 32 pixels. c. Velocity field with 0.25 overlapping on an interrogation window of 24 pixels. d. Signal to noise ratio with 0.66 overlapping on an interrogation window of 48 pixels. e. Signal to noise ratio with 0.25 overlapping on an interrogation window of 32 pixels. f. Signal to noise ratio with 0.25 overlapping on an interrogation window of 24 pixels. Adapted from Todaro (2020).

The region near the spray tip is of particular significance, yet the PIV results yielded lower Signal-to-Noise Ratio (SNR) values in this area. As shown in Figure 5, the SNR field for spray development with different windowing strategies was presented, and the velocity field underwent filtering strategies to eliminate regions with lower SNR. However, the filtering employed a threshold of 1.6 SNR, and the region near the spray tip could not achieve significantly higher SNR values.

Figure 6 illustrates the inlet air flow during the evolution of spray development for the PTV analysis, including pre-processed images and the vector field. The air movement is observed across four stages: recirculation, recirculation break, quasi-steady condition, and the end of injection.

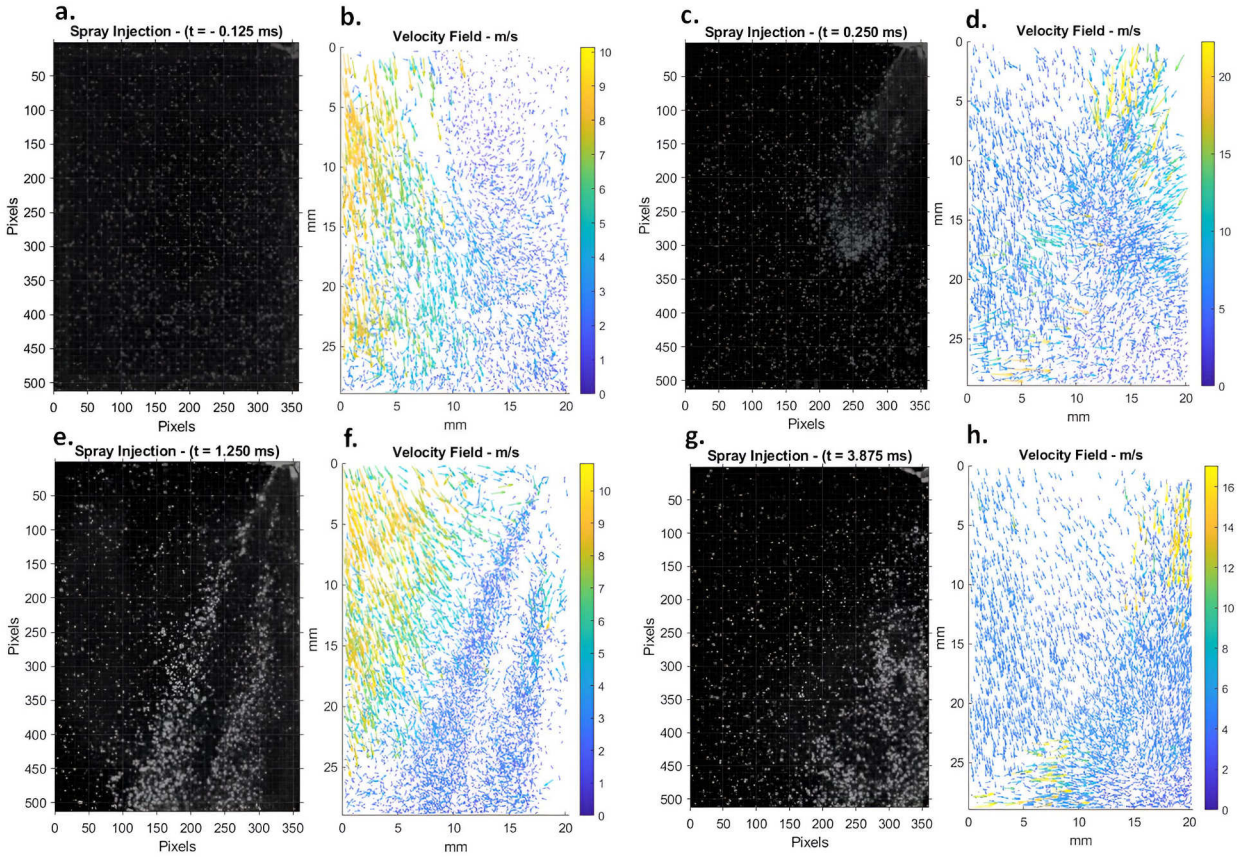


Figure 6. Spray development evolution for PTV analysis inside IESC and velocity field with injection pressure of 60 bar and air mass flow of 0.066 kg/s. a. t = $-0.125$ ms of SOI b. t = $-0.125$ ms of SOI. c. t = 0.250 ms of SOI. d. t = 0.250 ms of SOI. e. t = 1.250 ms of SOI. f. t = 1.250 ms of SOI. g. t = 3.875 ms of SOI. h. t = 3.875 ms of SOI.

In the first stage, depicted in Figures 6a and 6b, representing the recirculation stage at -0.125 ms before the start of ethanol injection (t = -0.125 ms SOI), recirculation occurs due to the IESC geometry and the change in the direction of inlet airflow, resulting from the flow around a bluff body. The region beneath the spray tip experiences lower pressures compared to the flow pressure, leading to two distinct regions in the vector field. To accommodate color restrictions, Figure 7 presents a profile graph orthogonal to the vertical axis of the spray, displaying the two vector components, $u$ and $v$. The first region exhibits downstream flow, primarily influenced by the chamber's air flow, with $u$ velocities ranging from -0.2 to 1.8 m/s. The second region is characterized by rotational flow below the spray tip, marked by the transition between positive and negative values of the vertical component, $v$, at $y = 50$ (2.83 mm) and $x > 200$ pixels. Here, $u$ velocities are -0.2 to 1.8 m/s. The inlet air flow alters the vertical component, shifting $v$ velocities from 8 to 10 m/s to 2 to 4 m/s. The $u$ velocity increases due to the vortical nature of the flow in this region. Beyond $x > 150$ pixels, vertical velocities tend toward zero or even become negative at $y = 50$ (2.83 mm) and $y = 150$ (8.49 mm), exhibiting upstream movement opposite to the vertical axis. At this injection stage, the velocity orientation closely resembles the findings from PIV, as modifications in the velocity fields result from pressure differentials acting in this region, with particles being uniformly distributed.

The second stage encompasses the initiation of ethanol injection, occurring from 0 to 0.250 ms. During this phase, the spray enters and elevates the vertical component. Figures 6c and 6d represent the recirculation break caused by the spray injection at t = 0.250 ms. Horizontal and vertical components are illustrated in Figure 7c and 7d. Both $u$ and $v$ components accelerate towards the spray boundary as a result of the air being displaced by the penetrating spray. The vertical component accounts for the majority of the velocity vector's value and dominates over the horizontal component. In this early injection phase, the spray pushes the remaining cluster downstream. Additionally, a vertical upstream component at the center axis of the spray suggests that the air is reacting to pressure differences caused by the spray injections at the shear layer droplet velocities and the center droplet velocities. During this phase, the $u$ velocities change, transitioning from negative values to positive between $x = 200$ and $x = 250$ pixels, and between $y = 150$ (8.49 mm) and $y = 250$

(14.15 mm) along the y-axis. Moreover, the $u$ magnitude at $y = 450$ (25.47 mm) increases from an average of 4.5 m/s to 7 m/s. This increase may be attributed to the injection displacing the air around the spray cone, creating an effect due to air mass continuity-equilibrium in the penetration zone. Additionally, the $v$ component at $y = 50$ (2.83 mm) experiences a notable increase in magnitude to 16 m/s at the shear layer region, marking a 52.4% increase. Other $y$ profiles do not exhibit a substantial increase in the $v$ component.

The third stage is characterized by the quasi-steady condition, spanning from 1.250 ms to 3.125 ms. During this phase, the ethanol spray exhibits very similar velocity distributions as the spray fully develops. This condition offers insights into the interaction between the inlet airflow colliding with the spray cone. The spray's momentum increases vector magnitudes near the spray cone and alters their direction. Additionally, a structure begins to emerge, affecting the airflow direction near the spray tip. These structures feature higher horizontal components compared to vertical ones.

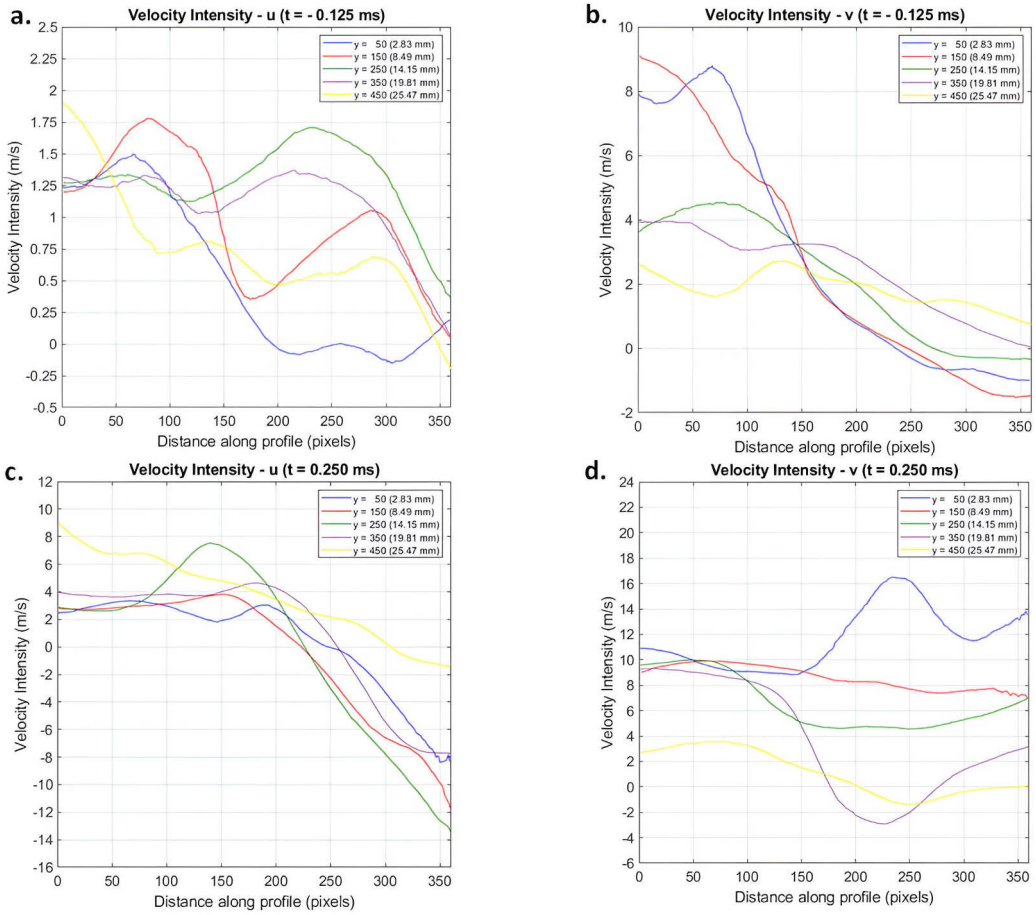


Figure 7. Velocity intensity profile orthogonal to $y$ axis along the spray development in $y = 50$, $y = 150$, $y = 250$, $y = 350$ and $y = 450$ pixels with PTV analysis. a. Horizontal velocity component in t = $-0.125$ ms. b. Vertical velocity component in t = $-0.125$ ms. c. Horizontal velocity component in t = $0.250$ ms. d. Vertical velocity component in t = $0.250$ ms.

The chosen Field of View (FOV) emphasizes the region near the spray tip. However, certain significant structures may remain obscured, particularly in a quasi-steady state. Additionally, recirculation structures discussed by Zhang *et al.* (2014) are dissipated by the vertical airflow injected into the chamber. The injector, being a multihole type, injects ethanol at velocities exceeding 20 m/s. As a result, ethanol injection is not uniform across the spray cone. The highest velocity magnitudes are observed during the quasi-steady condition and at the end of injection.

Figures 6e, 6f, 8a, and 8b represent the quasi-steady condition, displaying elevated velocity magnitudes near the spray tip due to the drag exerted by fast-moving droplets. The $u$ velocity of the air consistently decreases with increasing $y$. The peak, reaching 5 m/s, is situated between 100 to 150 pixels at $y = 50$ (2.83 mm). The increase in the $u$ component can be interpreted as a drag process of the air inside the internal spray cavities. These cavities extend throughout the spray development but are more pronounced near the spray tip, redirecting velocity vectors from the vertical to the horizontal direction.

The $v$ component enters the chamber with a velocity of 12 m/s and gradually decreases with increasing $y$, ultimately reaching 2 m/s. Near the shear layer, both $u$ and $v$ exhibit low-velocity intensity, primarily due to the reduced amount of light scattered by the droplets, which can hinder the PTV's ability to track particles effectively.

The fourth stage marks the end of injection, with the spray closure occurring 3 ms after Start of Injection (SOI). Figures 6g, 6h, 8c, and 8d depict the culmination of the injection process, where the surrounding air attempts to fill the void left by the spray's drag. In this zone, a portion of the inlet air changes its direction towards the center of the injector axis, resulting in horizontal components. Simultaneously, the spray continues to develop below the image frame, with air masses moving forward to interact with the other part of the inlet airflow.

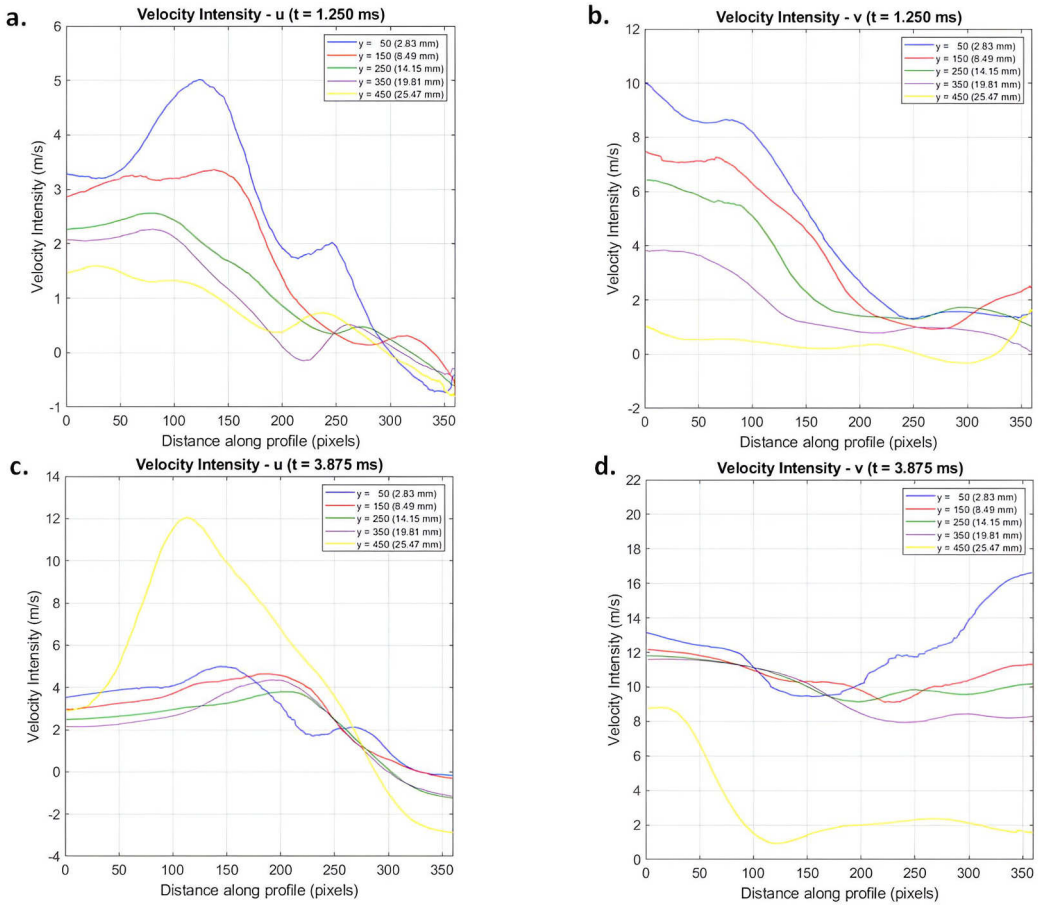


Figure 8. Velocity intensity profile orthogonal to $y$ axis along the spray development in $y = 50$, $y = 150$, $y = 250$, $y = 350$ and $y = 450$ pixels with PTV analysis. a. Horizontal velocity component in t = 1.250 ms. b. Vertical velocity component in t = 1.250 ms. c. Horizontal velocity component in t = 3.875 ms. d. Vertical velocity component in t = 3.875 ms.

The influence of the spray injection, especially after the spray closure, leads to elevated air velocities directed downstream. Velocities near the spray region gradually decrease, ultimately approaching zero. The recirculation zone reestablishes itself as the spray dissipates. The spray drag has a notable impact on the $u$ component, particularly at the interface of the two regions. At the center of the injector, magnitudes of $u$ remain near zero or even exhibit negative values.

In contrast, the vertical components near the spray tip reveal a strong airflow directed behind the spray. This phenomenon is linked to mass conservation after the needle valve closes. Higher injection pressures would logically result in higher velocity magnitudes. This indicates that the injector's structural configuration promotes the retention of air behind the spray, influenced by the experiment's geometry and inlet air velocities.

In comparison to the PIV analysis, the PTV analysis offers a reliable technique for investigating the continuous phase of a two-phase flow in a direct injection within a constant flow chamber. It effectively addresses the limitations of PIV in capturing information in specific regions of the air velocity field. However, PTV struggles to provide detailed insights into the air movement within the spray and near the shear layer.

The division of the flow into two distinct regions presents challenges, particularly in the shear layer, where the particle density gradient is higher. The chosen parameters for investigating the inlet air movement lead to particle images overlapping, making it more challenging to distinguish between different particles and accurately determine their positions. In contrast, the PIV analysis of the shear layer yields superior results compared to PTV. It can depict velocity gradients in this region and provide more reliable values for air movement within this noisy area.

### 3.2 Peak locking analysis

For the PTV measurements, a peak locking analysis was performed for each velocity field. To demonstrate the minimal presence of peak locking errors, the histograms exhibited a nearly flat distribution in sub-pixel displacement, with no distortion observed in the displacement histograms. Figure 9 illustrates the histograms of displacement in both pixels and sub-pixels for streamwise displacement.

For the PTV measurements in the present work, the values of PD range between 0.10152 and 0.18159, as defined in Section 2.2

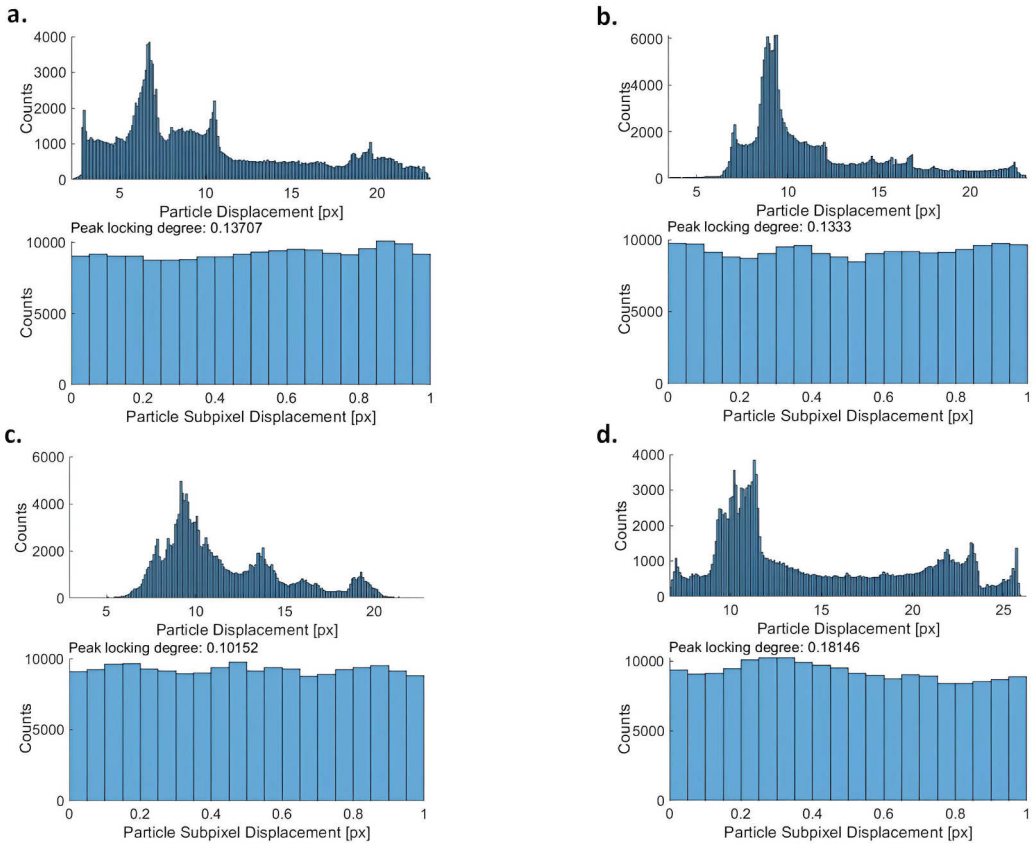


Figure 9. Histograms of the displacement in pixel and sub-pixel streamwise displacement for a. $t = -0.125$ ms b. $t = 0.250$ ms c. $t = 1.250$ ms d. $t = 3.875$ ms

## 4. SUMMARY AND CONCLUSIONS

In this study, we conducted a PTV measurement of the air surrounding an ethanol spray direct injection. PTV yielded coherent results for the inlet air movement and addressed certain noisy areas that were challenging for PIV analysis. While PIV employed relatively large interrogation windows with high overlap to achieve high spatial resolution, it encountered difficulties in analyzing the shear layer due to its noisy characteristics and particle overlap, a challenge better suited for PIV analysis.

However, the PTV approach allowed for a Lagrangian perspective of the air movement around the spray, revealing distinct stages of air motion. Notably, in the vicinity of the spray tip, where PIV faced challenges, PTV successfully matched particle densities and provided valuable insights into air movement in this critical area. We presented four distinct velocity field characteristics corresponding to different stages of spray development, and the calculated bias error was shown to be minimal.

## 5. ACKNOWLEDGEMENTS

The authors would like to express their gratitude to the Fundação de Amparo à Pesquisa do Estado de São Paulo (FAPESP) for their financial support (Grant No. 2021/017462), and extend special thanks to the Polytechnic School of the University of São Paulo.

## 6. REFERENCES

Aguera, N., Cafiero, G., Astarita, T. and Discetti, S., 2016. "Ensemble 3d ptv for high resolution turbulent statistics". *Measurement Science and Technology*, Vol. 27. ISSN 13616501. doi:10.1088/0957-0233/27/12/124011.

Baumgarten, C., 2006. *Mixture Formation in Internal Combustion Engines*. Springer Berlin Heidelberg. ISBN 3-540-30835-0. URL https://books.google.com.qa/books?id=ix8WRsXA-kEC.

Berti, R.d.C.R., 2018. *Interaction of turbulent structures with ethanol sprays in mixture formation processes in a constant-flow chamber.* Ph.D. thesis, Universidade de São Paulo, São Paulo. doi:10.11606/T.3.2018.tde-19092018-082453. URL http://www.teses.usp.br/teses/disponiveis/3/3150/tde-19092018-082453/.

Chen, J. and Katz, J., 2005. "Elimination of peak-locking error in piv analysis using the correlation mapping method". *Measurement Science and Technology*, Vol. 16, pp. 1605–1618. ISSN 09570233. doi:10.1088/0957-0233/16/8/010.

Dabiri, D. and Pecora, C., 2019. *Particle Tracking Velocimetry*. 2053-2563. IOP Publishing. ISBN 978-0-7503-2203-4. doi:10.1088/978-0-7503-2203-4. URL https://dx.doi.org/10.1088/978-0-7503-2203-4.

Duncan, J., Dabiri, D., Hove, J. and Gharib, M., 2010. "Universal outlier detection for particle image velocimetry (piv) and particle tracking velocimetry (ptv) data". *Measurement Science and Technology*, Vol. 21, p. 057002. ISSN 0957-0233. doi:10.1088/0957-0233/21/5/057002.

Fuchs, T., Hain, R. and Kähler, C.J., 2017. "Non-iterative double-frame 2D/3D particle tracking velocimetry". *Experiments in Fluids*, Vol. 58, No. 9, pp. 1–5. ISSN 07234864. doi:10.1007/s00348-017-2404-0.

Heyman, J., 2019. "TracTrac: A fast multi-object tracking algorithm for motion estimation". *Computers and Geosciences*, Vol. 128, pp. 11–18. ISSN 00983004. doi:10.1016/j.cageo.2019.03.007.

Janke, T., Schwarze, R. and Bauer, K., 2020. "Part2Track: A MATLAB package for double frame and time resolved Particle Tracking Velocimetry". *SoftwareX*, Vol. 11, p. 100413. ISSN 23527110. doi:10.1016/j.softx.2020.100413. URL https://doi.org/10.1016/j.softx.2020.100413.

Kahler, C.J., Scharnowski, S. and Cierpka, C., 2012. "On the resolution limit of digital particle image velocimetry". *Experiments in Fluids*, Vol. 52, pp. 1629–1639. ISSN 0723-4864. doi:10.1007/s00348-012-1280-x.

Melling, A., 1997. "Tracer particles and seeding for particle image velocimetry". *Measurement Science and Technology*, Vol. 8, pp. 1406–1416. doi:10.1088/0957-0233/8/12/005. URL https://dx.doi.org/10.1088/0957-0233/8/12/005.

Raffel, M., Willert, C.E., Scarano, F., Kähler, C.J., Wereley, S.T. and Kompenhans, J., 2018. *Particle Image Velocimetry A Practical Guide Third Edition*.

Raffel, M., Willert, C.E., Wereley, S.T. and Kompenhans, J., 2007. *Particle Image Velocimetry*. Springer Berlin Heidelberg, Berlin, Heidelberg. ISBN 978-3-540-72307-3. doi:10.1007/978-3-540-72308-0. URL http://link.springer.com/10.1007/978-3-540-72308-0.

Schanz, D., Schröder, A., Gesemann, S., Michaelis, D. and Wieneke, B., 2013. "'shake the box': A highly efficient and accurate tomographic particle tracking velocimetry (tomo-ptv) method using prediction of particle positions".

Shavit, U., Lowe, R.J. and Steinbuck, J.V., 2007. "Intensity capping: A simple method to improve cross-correlation piv results". *Experiments in Fluids*, Vol. 42, pp. 225–240. ISSN 07234864. doi:10.1007/s00348-006-0233-7.

Todaro, R.H., 2020. "Otimização de medidas PIV na interação de um spray de etanol com o ar circundante em uma câmara de fluxo contínuo".

Todaro, R.H., Pacífico, A.L., Amaral, R.D.L. and Krieger, C.G.F., 2020. "OPTIMIZATION OF PIV PROCESSING IN THE INVESTIGATION OF AN ISOTHERMAL ETHANOL SPRAY CHAMBER". *Brazilian Congress of Thermal Sciences and Engineering*.

Westerweel, J. and Scarano, F., 2005. "Universal outlier detection for piv data". *Experiments in Fluids*, Vol. 39, pp. 1096–1100. ISSN 07234864. doi:10.1007/s00348-005-0016-6.

Zabeu, C.B., 2019. "Investigações de estratégias de injeção e ignição de etanol em câmara de combustão de volume constante." doi:10.11606/T.3.2019.tde-31012019-072349. URL http://www.teses.usp.br/teses/disponiveis/3/3150/tde-31012019-072349/.

Zhang, M., Xu, M. and Hung, D.L., 2014. "Simultaneous two-phase flow measurement of spray mixing process by means of high-speed two-color piv". *Measurement Science and Technology*, Vol. 25. ISSN 13616501. doi:10.1088/0957-0233/25/9/095204.

## 7. RESPONSIBILITY NOTICE

The authors are solely responsible for the printed material included in this paper.